Thermodynamic properties and correlation functions of Ar films on the surface of a bundle of nanotubes

Nathan M. Urban,[*] Silvina M. Gatica,[†] and Milton W. Cole[‡]
Department of Physics, Pennsylvania State University,
University Park, Pennsylvania 16802-6300, USA

José L. Riccardo[§]
Departamento de Física, Universidad Nacional de San Luis, 5700 San Luis, Argentina

We employ canonical Monte Carlo simulations to explore the properties of an Ar film adsorbed on the external surface of a bundle of carbon nanotubes. The study is concerned primarily with three properties: specific heat $c(T)$, differential heat of adsorption q_d, and Ar-Ar correlation functions $g(\mathbf{r})$. These measurable functions exhibit information about the dependence of film structure on coverage and temperature.

I. INTRODUCTION

Considerable interest has been attracted recently to the properties of simple gases (noble gases and small molecules) adsorbed near bundles of carbon nanotubes.[1,2,3,4,5,6,7,8,9,10,11,12,13,14,15,16,17,18] This subject has been reviewed recently.[13,14] The adsorption of these gases can occur within the tubes only if they are open, which is possible either during the process of nanotube formation (e.g., when endohedral C_{60} molecules are formed),[15] or after chemical treatment to open the tubes.[16,19] The presence, or absence, of interstitial channel (IC) molecules is an open question in the case of an idealized bundle of identical tubes; there seems to be no doubt, however, that such IC adsorption occurs in laboratory samples of polydisperse tubes.[20] In contrast to variability in adsorption at these sites, the adsorption of gas on the external surface of the bundle is a ubiquitous phenomenon, in which the film coverage increases with the pressure (P) of the coexisting gas. In that exohedral environment, an adatom is strongly attracted to the groove region between two neighboring tubes; there, the film forms a quasi-one-dimensional phase. Further adsorption at low temperature (T) is predicted to manifest a so-called three-stripe phase of gas aligned parallel to the grooves.[21] At higher gas coverage (N), there occurs a two-dimensional monolayer phase, qualitatively analogous to that found on the graphite surface.[22,23] At even higher coverage, a multilayer film grows as P increases. There is an upper limit of total film coverage, set by the bundle's curvature;[24,25] this limit has yet to be explored.

This study extends a previous investigation[26] of the adsorption of Ar gas on the external surface of a nanotube bundle. Argon was chosen as a model adsorbate because its gas-gas interaction is well known, making it a standard fluid in the study of simple fluids. In the previous study, denoted I, we employed the grand canonical Monte Carlo simulation method to explore the evolution of the equilibrium film as a function of P and T. The present paper, stimulated by recent and proposed experiments, adds three results to those derived in the previous study. One property is the specific heat, $c(T)$, which is computed here from energy fluctuations, evaluated using simulations within the canonical ensemble. The second property is the differential heat of adsorption, $q_d = -(\partial E/\partial N)_T$, where E is the energy of the film. This quantity is closely related to another quantity, which is more often measured experimentally, the isosteric heat $q_{st} = (\partial(\ln P)/\partial\beta)_N$ [where $\beta = 1/(k_B T)$], by the relation[27] $q_{st} = q_d + k_B T$ (assuming an ideal gas coexisting with the film). The third property reported here is the anisotropic correlation function of the overlayer. This quantity is related by Fourier transform to results of diffraction experiments. With the exception of the isosteric heat calculated by Shi and Johnson,[20] none of these properties has been explored in simulation studies of films on nanotube bundles, prior to the present work.

The outline of this paper is the following. Section II summarizes our simulation methods. Section III reports results for the density and correlation functions. Section IV presents results for the thermodynamic properties, c and q_d. Section V summarizes our results.

II. COMPUTATIONAL METHODS

When not explicitly contradicted in this paper, it may be assumed that the physical system and computational method are as described in I. The primary model system is a bundle of infinitely long, cylindrically symmetric carbon nanotubes of identical radii equal to 6.9 Å. Only two adjacent nanotubes on the external surface of the bundle are simulated. The y axis is parallel to the nanotubes, and the z axis is directed away from the surface of the bundle. Periodic boundary conditions are imposed in the x and y directions (approximating the surface of the bundle as an infinite plane of nanotubes); reflecting boundary conditions are imposed in the z direction. The unit simulation cell, whose volume contains half of each of the two adjacent nanotubes with the groove in between them

at the center, is 17 Å in the x direction, 34 Å in the y direction, and 40 Å in the z direction.

The simulations were done in the canonical ensemble, rather than the grand canonical ensemble more commonly used in adsorption simulations, in order to facilitate the calculation of the heat capacity. Two Markov Chain Monte Carlo simulation methods were used, the Metropolis algorithm[28,29] and the Wang-Landau algorithm.[30,31,32] The Metropolis algorithm was used to calculate configurational observables, such as density distributions and correlation functions. The Wang-Landau algorithm was used to calculate thermodynamic observables expressible in terms of ensemble averages or their derivatives, such as specific and isosteric heat, for certain N; the Metropolis algorithm was used to determine the full N dependence.

The Metropolis algorithm proposes new configurations and accepts them with a probability equal to $\min\{1, P(\mathbf{x}')/P(\mathbf{x})\}$, where $P(\mathbf{x})$ and $P(\mathbf{x}')$ are the probabilities of the old and new configurations $\mathbf{x}$ and $\mathbf{x}'$; this acceptance rule causes the random walk to converge to the probability distribution $P(\mathbf{x})$. By choosing $P(\mathbf{x})$ proportional to the Boltzmann factor $\exp[-\beta U(\mathbf{x})]$, where $U(\mathbf{x})$ is the potential energy of the configuration, the Metropolis algorithm uniformly samples configuration space. For the Metropolis simulations of each (N, T), 4×10^7 Monte Carlo moves were discarded during the initial equilibration to converge the algorithm to the Boltzmann distribution, then 4×10^6 moves were generated, from which 10^4 samples were drawn to perform simulated measurements of system observables.

The Wang-Landau algorithm, like the Metropolis algorithm, also proposes and accepts configurations with a probability equal to $\min\{1, P(\mathbf{x}')/P(\mathbf{x})\}$. However, it chooses $P(\mathbf{x})$ to be proportional to $P[U(\mathbf{x})] = 1/g[U(\mathbf{x})]$, where $g(U)$ is the (relative) density of states, thus uniformly sampling *energy* space (instead of configuration space, as in the Metropolis algorithm). It dynamically refines its estimate of the density of states by counting each visit to a state of a given energy U (or, rather, within a small range of energies $U \in [U_i - \epsilon/2, U_i + \epsilon/2]$ about an energy bin U_i of width ϵ), and multiplies its running estimate of $g(U_i)$ by a constant factor f. It continues the random walk until each energy is visited approximately uniformly (a "flat histogram" of visits in energy space), whereupon it reduces the factor $f \rightarrow f^{1/2}$ and starts another iteration. The algorithm terminates when f is reduced to a preset minimum greater than unity, with values closer to unity yielding more accurate estimates of the density of states.

Once an estimate of $g(U)$ is produced, it can be used to calculate the partition function directly

$$Z \sim \int d\mathbf{x}\, e^{-\beta U(\mathbf{x})} \approx \sum_i g(U_i) e^{-\beta U_i}. \qquad (1)$$

Thermodynamic quantities can then be calculated from the partition function, as usual. One advantage of the Wang-Landau algorithm over the Metropolis algorithm (and the main reason for using it for this study) is that, because temperature dependence appears only in the Boltzmann weight $\exp(-\beta U)$ and not in the density of states $g(U)$ itself, a single simulation of $g(U)$ can calculate thermodynamic observables for all temperatures at once.

Some modifications and improvements to the original published Wang-Landau algorithm were implemented. Boundary effects were properly handled.[33] To adapt the original lattice-based algorithm to continuum systems, preliminary Metropolis runs at low temperature were performed to estimate a lower bound on the energy bins (i.e., the ground state energy).[34] The simulation can also become trapped for long periods of time in regions of high degeneracy, so that energies with small $g(U)$ go a long time before being revisited. To remedy this, the energy bins can be broken up into overlapping subranges; ergodicity can be achieved more rapidly if the interval of energies to be traversed is smaller. Separate simulations are performed in each subrange, producing independent estimates of $g(U)$. Some care must be taken in combining them into an estimate of $g(U)$ over the full energy range: because each simulation calculates only the *relative* density of states, the estimates will not generally match up at the boundaries of the subranges. To overcome this, each subrange estimate of $g(U)$ is rescaled by a constant factor that minimizes the least-square error in $\log g(U)$ wherever two neighboring subranges overlap in energy.[34] This corresponds to choosing normalizing factors C_n that minimize the sum $\sum_i \{\log[g_n(U_i)/C_n] - \log[g_{n-1}(U_i)]\}^2$ over the overlapping bins U_i (where g_n denotes the density of states simulated over subrange n), and then rescaling $g_n(U)$ by C_n.

For the Wang-Landau simulations of each N, 1500 equal-sized energy bins were used in a range $[U_{\min}, 0]$, where $U_{\min}$ is the ground state energy. The 1500 bins were divided into four overlapping subranges, simulated separately, consisting of the bins numbered 1–150, 76–787, 713–1425, and 1351–1500. A histogram was considered "flat" when the number of visits to any particular energy bin was less than $\pm 20\%$ the average number of visits to any bin. The minimum f factor was $f_{\min} = 1 + 10^{-5}$.

III. CORRELATION FUNCTIONS

For the purposes of this paper, the three-dimensional pair correlation function is defined as the probability density $g(\mathbf{r})$ that two particles are separated by a relative displacement $\mathbf{r}$. Its projection $G(x, y) \equiv \int dz\, g(\mathbf{r})$ into the xy plane is depicted in Fig. 1. The contours become wider and more irregular at higher temperatures, as the particles are thermally excited out of their well-defined low temperature sites.

In the top pair of panels, one observes the nearly periodic, quasi-one-dimensional (1D) order within the groove. As studied recently in connection to nanotube
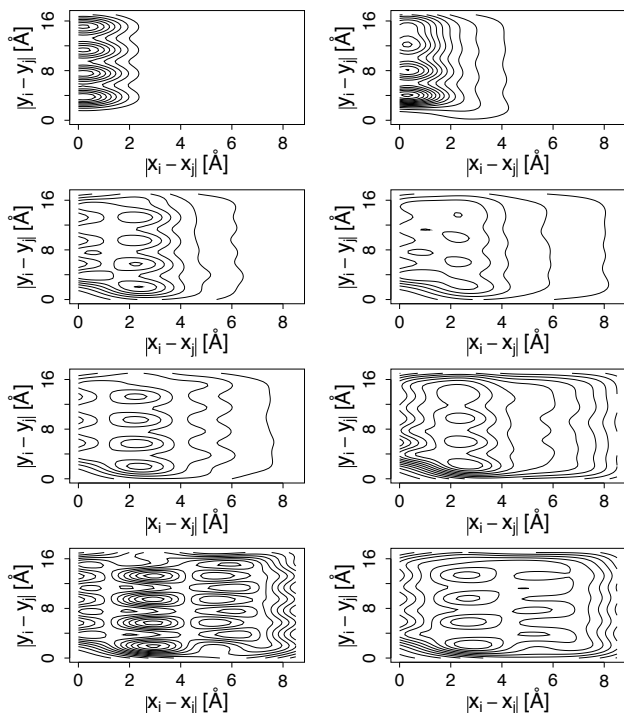
FIG. 1: Equiprobability contour plots of the projection into the xy plane of the pair correlation function, $G(x, y)$ for, from top to bottom, $N = 9$ (groove), $N = 18$, $N = 27$ (three-stripe), and $N = 54$ (monolayer), at $T = 60$ K (left) and $T = 90$ K (right). Distances are in angstroms. Note that the vertical axis scale is compressed relative to the horizontal.

adsorption,[35,36,37,38,39,40] this phase may undergo a phase transition due to the weak interactions between particles in neighboring grooves. In the second pair of panels, one observes that the correlations within the three-stripe phase are weaker and even more T dependent than those in the groove phase. At 90 K, at higher coverage (seen in the middle four panels), the stripes are not as straight, primarily due to transverse excitation (as discussed in Sec. IV C). Note that the half-filled stripe case ($N = 18$) is somewhat less ordered than the completely filled three-stripe case ($N = 27$), as is expected. The bottom panels of Fig. 1 exhibit a highly correlated anisotropic two-dimensional (2D) solid at 60 K, the order of which washes out nearly completely by 90 K, as the monolayer melts.

Previous experimental studies of Ar adsorption onto planar graphite[41,42,43,44] found that the melting temperature depends on density, starting near 55 K at low density, and increasing with density. Although the system studied here differs from that experiment in geometry, we expect the melting temperature of the monolayer in our system to similarly increase with density. The corrugation of the nanotube bundle should elevate the melting temperature somewhat compared to a planar surface, as the grooves will serve to more strongly confine the film's structure.

Bienfait *et al.* have measured diffraction patterns for

Ar on nanotube bundles.[2] Probably due to heterogeneity (for which there exists evidence in bare surface diffraction), the diffraction data are not easily interpreted. There is, however, definite evidence of 1D interatomic spacing (i.e., a peak at wave vector $q = 17/$nm) at low coverage and 2D close-packed spacing (peak near $20/$nm).

IV. HEAT CAPACITY

A. Overview

The isochoric specific heat, $c(T) = (\partial E/\partial T)_V/N$, i.e., the heat capacity (per particle) at constant volume, was calculated from ensemble averages. It is known[45] that the heat capacity can be given in terms of energy fluctuations, $(\partial E/\partial T)_V = (\langle E^2 \rangle - \langle E \rangle^2)/(k_B T^2)$, where $\langle \cdot \rangle$ denotes an expectation taken over the canonical ensemble. The equipartition theorem gives the kinetic energy contribution of $\frac{1}{2}k_B$ per degree of freedom to the specific heat, yielding a total $c(T) = \frac{3}{2}k_B + (\langle U^2 \rangle - \langle U \rangle^2)/(N k_B T^2)$. Given the density of states $g(U)$ calculated with the Wang-Landau algorithm, the expectations may be calculated from $\langle U \rangle = Z^{-1} \sum_i U_i \, g(E_i) \exp(-\beta U_i)$, and similarly for $\langle U^2 \rangle$. The heat capacity was also estimated directly from the derivative $(\partial E/\partial T)_V$ by means of a finite difference approximation. These latter estimates, while consistent with the fluctuation estimates, were "noisier" and are not considered further in this paper.

The simulated $c(T)$ for the groove, three-stripe, and monolayer phases is shown in Fig. 2. Note that the overall trend is for $c(T)$ to have a remarkably high value, in the range 3–7 Boltzmanns, much higher than might be expected from simple quasi-one-dimensional and two-dimensional models. We do not have a detailed quantitative model to explain all of the observed features, but we can give a qualitative explanation of its behavior. The explanations are justified by examining the probabilities of finding particles at given energies in the external potential, Fig. 3, indicating the fraction of particles that are in the groove, stripes/monolayer, etc. (quantified in Table I).

B. Low density

Consider first the low-density limit.[47] At low temperatures, the specific heat is near 2.5 Boltzmanns. This is to be expected: the three kinetic degrees of freedom each contribute the usual $1/2$ Boltzmann; the two transverse dimensions, for which the external potential is approximately harmonic at its minimum at the center of the groove, each contribute another $1/2$ Boltzmann. As the temperature increases, a peak in the specific heat occurs near 170 K when substantial numbers of adatoms are promoted out of the groove and into monolayer sites
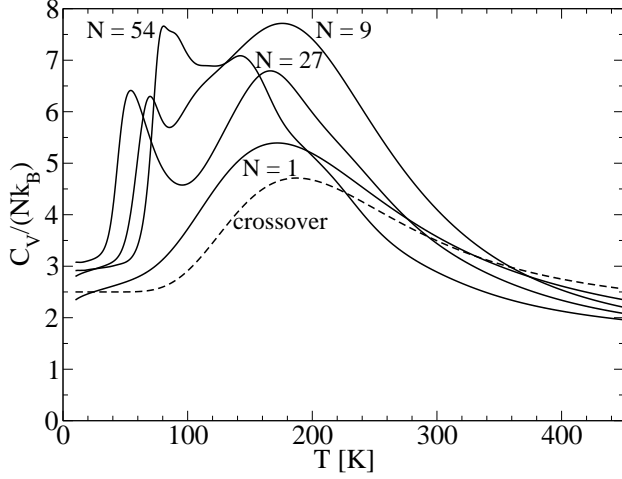
FIG. 2: The dimensionless specific heat $c(T)/k_B$ of the low-density limit ($N = 1$); the groove ($N = 9$), three-stripe ($N = 27$), and monolayer ($N = 54$) phases; and the theoretical prediction of the low-density limit given by the dimensional crossover model (discussed in the text).
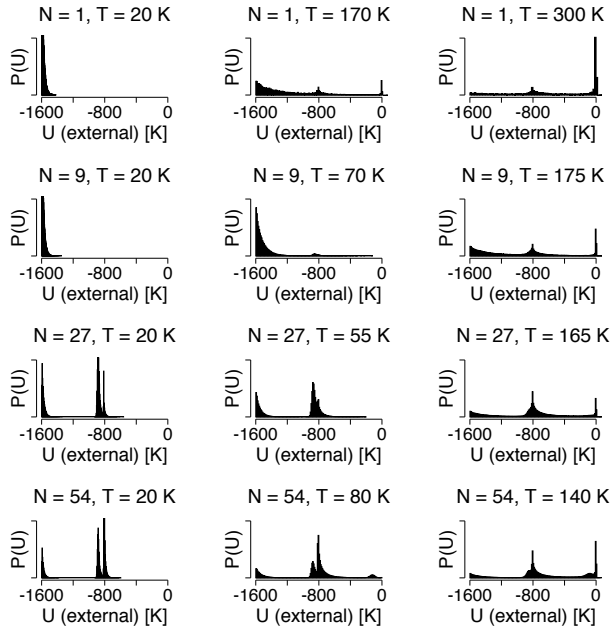

FIG. 3: The relative probability $P(U_{ext})$ of finding a particle at an external potential of U_{ext}, for the low-density limit ($N = 1$), and the groove ($N = 9$), three-stripe ($N = 27$), and monolayer ($N = 54$) phases, for various temperatures.

elsewhere on the surface of the nanotubes (see Table I). As $T \to \infty$, the adatoms desorb from the surface altogether, and $c(T)$ approaches the 3/2 Boltzmanns of the three kinetic degrees of freedom of a pure vapor. (This will be the case for all other densities as well, in the high-T limit.)

These conclusions are corroborated, as mentioned, in the first row of Fig. 3; these results, in the low-density

N	T (K)	% groove	% monolayer	% vapor
	20	100	0	0
1	170	61	31	7
	300	14	35	51
	20	100	0	0
9	70	93	6	0
	175	43	42	15
	20	33	67	0
27	55	33	67	0
	165	22	60	18
	20	17	83	0
54	80	17	77	7
	140	14	54	32

TABLE I: Percentage of particles in the groove (-1600 K $< U_{ext} < -1200$ K), monolayer (-1200 K $< U_{ext} < -400$ K), and vapor ($U_{ext} > -400$ K) regimes, for the low-density limit ($N = 1$), and the groove ($N = 9$), three-stripe ($N = 27$), and monolayer ($N = 54$) phases, for various temperatures.

limit, can also be understood by examining the so-called "volume density of states"[46] $f(U)$, defined such that $f(U) dU$ is the volume of space bounded by infinitesimally separated isopotential surfaces, $U < U_{ext} < U + dU$. This function is related to the energy probability density $P(U)$ in Fig. 3 at low density by $P(U) = \rho f(U) \exp(-\beta U)$, where ρ is the number density of particles. By dividing an estimate of $P(U)$ at a given temperature (here, $T = 300$ K) by the exponential Boltzmann factor, we obtain an estimate proportional to the volume density of states $f(U)$, depicted in Fig. 4.
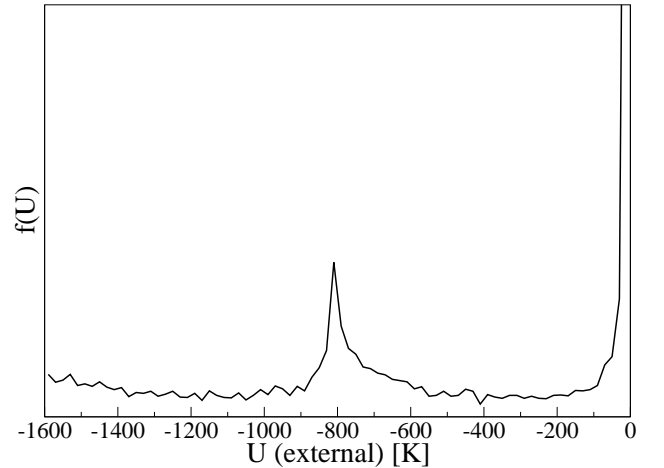

FIG. 4: The function $f(U)$ (unscaled), giving the volume of space $f(U) dU$ enclosed within a range of external potential energy $[U, U + dU]$.

The qualitative form of this figure can be explained by appealing to a previously studied analytic model, the dimensional crossover model.[47] This exactly soluble model ignores interparticle interactions (an assumption

appropriate for the low-density limit) and treats the nanotube bundle as consisting solely of two regions, a one-dimensional groove region approximated by a harmonic potential in the two transverse dimensions, and a two-dimensional planar monolayer region approximated by a harmonic potential normal to the surface. Evaporation from the monolayer to vapor is neglected. Its (configurational) partition function is given by

$$Z_{\text{crossover}} = \int_{\text{groove}} d^2r\, e^{-\beta[V_g + (1/2)\alpha r^2]}$$
$$+ L_s \int_{\text{mono}} dz\, e^{-\beta[V_m + (1/2)k_m z^2]}, \quad (2)$$

where the parameters $V_g = -1671$ K, $\alpha = 4898$ K/Å^2, $V_m = -853$ K, and $k_m = 4792$ K/Å^2 were determined by a fit to the external potential, $L_s = 18$ Å is the approximate width of the monolayer region in the transverse direction, and integrations were taken over regions extending 2 Å away from the groove minimum and 1 Å away from the monolayer minimum.

For the low energies dominated by the groove phase, the crossover model approximates the external potential as $U = V_g + \frac{1}{2}\alpha r^2$. The cylindrical volume enclosed by an isopotential goes like $V \sim r^2$, and $f(U) = dV/dU = (dV/dr)/(dU/dr)$, which is a constant; indeed, the $f(U)$ calculated in Fig. 4 is nearly constant at low energies. For the monolayer region, close to the potential minimum, $U = V_m + \frac{1}{2}k_m z^2$. The rectangular volume enclosed by an isopotential goes like $V \sim z$, and $f(U) = (dV/dz)/(dU/dz)$, which goes like $z^{-1} \sim (U - V_m)^{-1/2}$ for $U > V_m$. This divergence in the model accounts qualitatively for the peak in $f(U)$ just above the monolayer energy of about -800 K. For high energies dominated by the vapor phase, we can treat the substrate as a semi-infinite rectangular volume, and approximate the external potential by a long-distance (r^{-6}) Lennard-Jones potential integrated over this region, which yields $U \sim -z^{-3}$. Then $f(U)$ will go like $z^{-4} \sim (-U)^{-4/3}$, qualitatively accounting for the sharp rise in $f(U)$ as $U \to 0$.

Given the volume density of states $f(U)$, we can then obtain the energy probability density $P(U)$ at any other temperature by scaling this temperature-independent function by the appropriate Boltzmann weight. In particular, the three columns of the first row of Fig. 3 are just the function in Fig. 4 scaled by Boltzmann factors $\exp(-\beta U)$ that decay with decreasing rapidity as T increases (β decreases). The groove is highly populated at low temperatures (large β) when the exponential damping is great enough to suppress population at higher energies. The monolayer becomes populated at intermediate temperatures when the damping is no longer sufficient to suppress the peak in $f(U)$ that occurs at the monolayer energy (-800 K), and the vapor becomes populated at still higher temperatures (small β) when the damping fails to suppress the rapid increase in $f(U)$ towards 0 K.

The partition function of the crossover model can also

be used to calculate the specific heat directly. As seen in Fig. 2, the correspondence between the prediction of this analytic approximate model and the simulated full model is quite good.

C. Higher coverage

Next, consider the groove phase. At low temperatures, the specific heat is near 3 Boltzmanns. A contribution of 2.5 Boltzmanns is accounted for by the same argument as for the low density limit. Unlike the low density limit, however, the groove phase is densely packed with adatoms, and interparticle interactions must be considered. An additional 1/2 Boltzmann arises from confinement in the longitudinal dimension, for which the Ar-Ar interaction potential is approximately harmonic at its minimum when the adatoms are stably distributed in equilibrium. As the temperature increases, evaporation out of the groove begins. At $T \approx 70$ K, evaporation is great enough to excite adatoms out of the groove; while not many of these atoms reach the monolayer region (Table I), there is still a large change in potential energy for a small increase in temperature, and thus a large specific heat. The specific heat then decreases slightly with increasing temperature, since the change in energy is not as large once the initial adatoms have begun to be promoted. This low-temperature peak is not present in the low-density case because, as seen in both Table I and Fig. 1, the adatoms are not spread transversely as greatly about the immediate groove region at low temperatures in the low-density case as they are in the groove case. However, in a manner qualitatively analogous to the low-density limit, an additional, larger peak in the specific heat is found at still higher temperatures ($T \approx 175$ K), mostly from promotion from the groove into the stripes and the rest of the monolayer.

Like the groove phase, the three-stripe phase starts out at 3 Boltzmanns at low temperatures, similar to the groove phase, except that the 1 Boltzmann from external potential confinement in the transverse plane is replaced by 1/2 Boltzmann from external potential confinement normal to the surface, and 1/2 Boltzmann from interparticle confinement along the surface in the transverse plane. The specific heat peaks near $T = 55$ K; this is not due to a significant fraction of particles being promoted from the groove to the stripes, as one might expect, but rather to a wider range of energies within the stripe/monolayer region, and promotion from the stripes to the rest of the monolayer; see Fig. 3 and Table I. It peaks again near $T = 165$ K, with as the groove empties into the stripes and monolayer, as well as the beginning of evaporation off the surface.

The monolayer phase also starts out at 3 Boltzmanns at low temperatures, for reasons analogous to the three-stripe phase. At higher temperatures, there is a peak in the specific heat near $T = 80$ K which, like the three-stripe peak, is largely due to a broadening of the parti-

cles across a range of energies in the monolayer region, as well as some promotion from the monolayer to the bilayer (Fig. 3). Another peak appears near $T = 140$ K, corresponding to evaporation out of the monolayer into the bilayer, and to vapor.

D. Further results

The N dependence of several isotherms is displayed in Fig. 5. Of particular note is the rapid rise in the specific heat near $N \sim 8$, just before groove completion, as T goes from 60 to 90 K. This is attributed to promotion out of the groove. Similarly, near monolayer completion the marked increase in c with T is attributed to thermal promotion out of the monolayer.
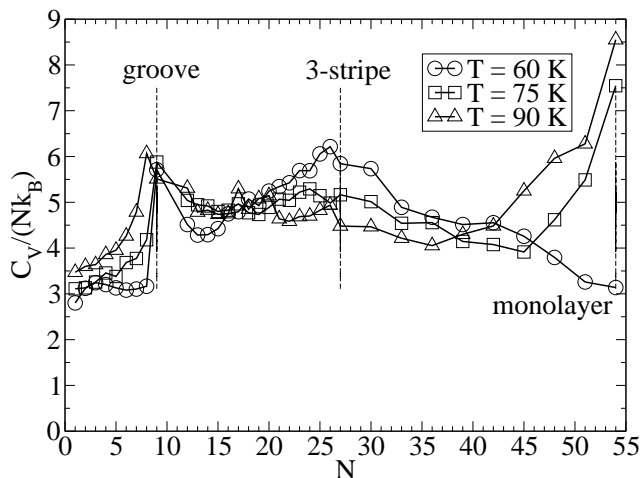

FIG. 5: The dimensionless specific heat $c(T)/k_B$ as a function of density, at $T = 60$, 75, and 90 K.

It is also illuminating to study the differential heat of adsorption, $q_d(N) = -(\partial E/\partial N)_T$, the energy required to adsorb an additional particle onto the surface at constant temperature. The differential heat is related to the heat capacity at constant density, $C_N = (\partial E/\partial T)_N$, by a Maxwell relation derived from the total derivative $dE = (\partial E/\partial T)_N \, dT + (\partial E/\partial N)_T \, dN$, which yields

$$\left(\frac{\partial C_N}{\partial N} \right)_T = - \left(\frac{\partial q_d}{\partial T} \right)_N . \tag{3}$$

(Note that $C_N = C_V$ in the canonical ensemble.)

The differential heat of adsorption is summarized in Fig. 6. At low densities, the differential heat is near the minimum of the external groove potential ≈ -1600 K, becoming slightly larger at lower temperatures. Both this value and the T dependence at low N can be understood from the low-density equation of state, $U/N = V_g + \frac{5}{2}k_B T$. As additional particles are added, the energy for each additional particle is reduced by slightly more than this amount, to include the interaction energy.

As the groove phase is approached, the groove becomes tightly packed and the interaction energy becomes significant, so that adding an additional particle reduces the energy by the external groove potential plus the Lennard-Jones well depth, $\epsilon \approx -120$ K for Ar. The difference in $q_d(N)$ between low and high temperatures is particularly large just before the groove phase, which in accordance with Eq. (3) corresponds to the steepest increase in heat capacity as seen in Fig. 5; at the $N = 9$ groove phase itself, where the heat capacity peaks with increasing N, we see correspondingly little difference in the differential heat at various temperatures. At the other extreme, near monolayer completion, a similar T dependence is observed. The large decrease in q_d with increasing T is consistent with Eq. (3) and Fig. 5; the latter shows a large value of dC/dN except below 60 K. The explanation is monolayer-to-bilayer promotion above 60 K.
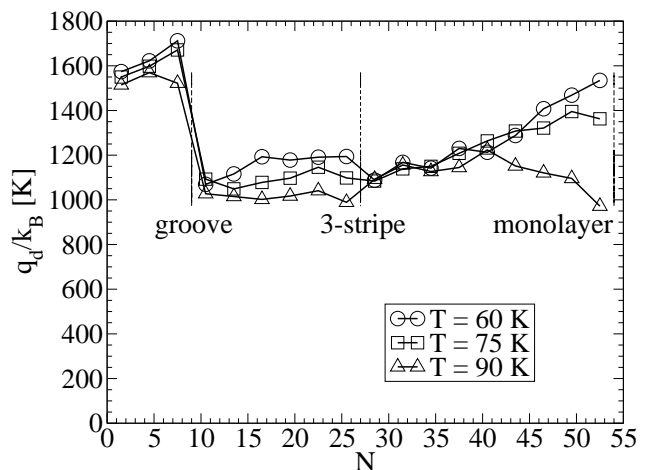

FIG. 6: The differential heat of adsorption $q_d(N)/k_B$ at $T = 60$, 75, and 90 K. [Shift each curve upwards by its temperature T to obtain the isosteric heat $q_{st}(N)/k_B$.]

Experimental measurements of isosteric heat for argon on nanotube bundles have been reported by Wilson et al.,[11] Talapatra, Rawat, and Migone,[7] Jakubek and Simard,[4] and Bienfait et al.;[2] grand canonical Monte Carlo simulations have been published by Shi and Johnson.[20]

The isosteric heat calculations of Shi and Johnson for adsorption of Ar on a homogeneous bundle at 90 K agree closely with our results, with a peak of $q_{st} = 14$ kJ/mol just before the groove phase, corresponding to our peak of 1650 K. Past the groove phase, their calculated isosteric heat drops and remains constant with coverage, slightly below 10 kJ/mol, corresponding to our nearly constant value near 1200 K.

Shi and Johnson compared their calculations to the experimental results of Wilson et al. and Talapatra et al., and since we agree with those calculations, we will briefly summarize their conclusions. Our calculations agree with both experiments at higher coverage, beginning at the

three-stripe phase, but their isosteric heats at lower coverage are dramatically greater than ours, as large as 18 kJ/mol ($\sim$ 2200 K) at low coverage. We ascribe this discrepancy with experiment to our neglect of bundle heterogeneity, following Shi and Johnson, whose simulations of heterogeneous bundles agreed well with both experiments.

In contrast, the isosteric heats measured by Jakubek and Simard agreed well with our simulations, with a peak of 137 meV ($\sim$ 1600 K) near the groove, descending to plateau of 106 meV ($\sim$ 1200 K) through to monolayer coverage. This agreement with our calculations suggests that their bundles were more homogeneous than those studied in the other two experiments. It should be noted, however, that their isosteric heat continues to decrease as coverage increases, whereas our isosteric heat appears to rise slightly as the monolayer is approached. The isosteric heat of Wilson $et\ al.$ also drops past the monolayer.

Like the other experiments, the results of Bienfait $et\ al.$ for Ar exhibit two plateaus in the dependence of the isosteric heat on coverage. The lowest coverage data yield $q_{st} = 15$ kJ/mol, or about 1800 K. Our predicted value in this range is of order 1650 K. The higher coverage, broad plateau corresponds to a measured $q_{st} = 1200$ K, which agrees well with the value we find for the three-stripe phase. However, the data at monolayer coverage continue to decrease, while ours appear to increase, as noted. Another area of disagreement is the extent, in coverage, of these plateaus. In the data, the second plateau extends over a coverage range comparable to that of the first plateau. Our calculations, instead, find that groove region of high q_{st} extends over just one-sixth of the range of the combined three-stripe plus monolayer regime (grouped together because of similar values of q_{st}). This discrepancy may be attributed to the role of large interstitial cavities within the bundle, as argued by Bienfait $et\ al.$

V. SUMMARY AND CONCLUSIONS

Our results are intended to stimulate further experimental studies of this system and analogous systems involving other gases on nanotube bundles. We have investigated the variation of thermodynamic properties with T and N. One of the more interesting general results is that the specific heat is typically larger than might have been expected from either simple models used to treat these systems (either independent particles or a solid)[18] or from experimental results for films on graphite.[22] For most conditions studied here, the specific heat exceeds three Boltzmanns, with average values in the range four to five Boltzmanns. In contrast, the specific heat of independent particles[47] in this environment is less than three Boltzmanns, except at high T (above 100 K), when the particles are excited out of the groove. The large values found in these simulations arise from the fact that the highly corrugated po-

tential surface presents a sequence of excitation steps (groove→three-stripe→monolayer→ $\cdots$ →vapor), each of which enhances the specific heat.

The temperature dependence of the specific heat shows a characteristic double-peak structure. All densities show a large peak near 175 K, corresponding to promotion of adatoms out of the groove into the monolayer region. The groove, three-stripe, and monolayer phases show an additional peak at lower temperature, corresponding to a thermal broadening in the range of external potential energies of the particles, rather than to any significant promotion of particles into qualitatively different regions.

Other principal results involve the relation between the evolution of film structure (with increasing N) and the corresponding thermodynamic and correlation functions. As the groove begins to fill (N approaching 9), the heat capacity shows a dramatic jump as a function of coverage. Consistent with the Maxwell relation, Eq. (3), the differential heat decreases with T at that point (Fig. 6). Analogous behavior occurs near completion of the three-stripe phase, near $N = 27$.

Our study has been fully classical, but the temperatures beneath which quantum effects become significant can be estimated.[47] We estimate that quantum effects can be ignored above about 80 K (see Appendix A). This is a higher temperature than some of the important structure in the heat capacity—the first peak in the heat capacity occurs at or below this temperature. Modifications to the heat capacity from quantum mechanics at very low energies are given by Debye theory:[18,48,49,50] we expect that $c(T) \to 0$ as $T \to 0$, and $c(T) \propto T^d$, where $d \sim 1$ for the groove and $d \sim 2$ for the monolayer, if the density is high enough to form a bulk phase. To evaluate quantum effects accurately would require application of the path integral Monte Carlo method to the problem.[51]

We note, also, that an experimental heat capacity cell has a volume on the order of 1–10 cm^3, whereas our simulation volume was on the order of 10^{-20} cm^3. Our simulation, focusing on small volume nearer the adsorbed film, thus ignores almost all of the volume in which desorption into vapor can occur. This causes the simulation to underestimate the heat capacity that will be experimentally measured. The effects of desorption cannot be ignored when the number of atoms in the vapor starts to approach the number of atoms in the film; this occurs at roughly 25–50 K (see Appendix B).

Particularly interesting results from the correlation function studies include the reduced longitudinal correlations in the groove and striped phases as T rises above 60 K. These results would be amenable to testing by diffraction experiments even if the samples included a randomly oriented batch of nanotubes; this is a familiar problem dealt with in powder averaging of small-sample experiments.

This paper studied a system of identical nanotubes. The sensitivity of $c(T)$ to nanotube heterogeneity, with an asymmetric groove region between nanotubes of different sizes, is a potentially interesting subject for future

investigation.[20]

APPENDIX A: QUANTUM EFFECTS

The upper bound on the temperature at which quantum effects must be considered is dominated by the physics of the deepest energy well, i.e., the groove. We can obtain one estimate by considering the minimum energy of longitudinal phonons in the groove in Debye theory, $\hbar\omega_D$, where $\omega_D = \sqrt{k/m}$ and $k = 2^{8/3}(9\epsilon/\sigma^2)$ is the force constant of a quadratic approximation to the minimum of the Ar-Ar interaction potential, a 12-6 Lennard-Jones potential $U_{\text{int}} = 4\epsilon[(\sigma/r)^{12} - (\sigma/r)^6]$, with $\sigma = 3.4$ Å, $\epsilon = 120$ K for Ar. The corresponding energy is 27 K. This estimate considers only Ar-Ar interactions and ignores the external potential; we can obtain a complementary estimate by ignoring the interactions and considering only the external potential. We return to the crossover model of the groove, outlined in Sec. IV, as a two-dimensional harmonic oscillator with a force constant $\alpha = 4898$ K/Å^2. Treating it now as a *quantum* harmonic oscillator, it is excited at an energy $\hbar\omega_\perp$, where $\omega_\perp = \sqrt{\alpha/m}$ and m is the atomic mass of argon. The corresponding energy of this second estimate is 77 K. Taking the larger of the two as a conservative estimate, we expect that quantum effects can be ignored above about 80 K.

APPENDIX B: EFFECTS OF DESORPTION

We can estimate the temperature at which desorption into the full volume of an experimental cell becomes significant, by determining when the ratio N_v/N_m of atoms in the vapor to atoms in the monolayer becomes significant. Extending the crossover model, we can consider the monolayer and vapor phases as separate systems, the monolayer modeled as a surface with a harmonic normal potential, and the vapor modeled as a free gas. The ratio N_v/N_m is then given by the ratio of their respective partition functions

$$\frac{N_v}{N_m} = \int_{\text{cell}} dz \Big/ \int_{\text{mono}} dz\, e^{-\beta[V_m + (1/2)k_m z^2]}. \quad \text{(B1)}$$

We take the first integral between zero and the cell height, h; the second integral may be safely taken between zero and ∞, in the interests of finding an analytic solution. This gives

$$\frac{N_v}{N_m} = \frac{h}{\sqrt{\pi/(2\beta k_m)}}\, e^{-\beta V_m}. \quad \text{(B2)}$$

The fraction of atoms in the vapor above which desorption should be considered "significant" is ambiguous, but we might take it to be 10%–20%. Solving Eq. (B2) for β, using $h = 1$ cm and the values for V_m and k_m found in Sec. IV B, this corresponds to a temperature in the range of 25–50 K.

This calculation neglects interparticle interactions. Their inclusion would lower the estimate of the temperature at which desorption from the monolayer into vapor becomes significant, analogously to how the evaporation from the groove to the monolayer takes place at a lower temperature when the groove is packed—the interacting case—than when it is sparsely populated and the adatoms are effectively noninteracting. This is supported by the data in Table I: more groove→monolayer promotion occurs for $N = 9$ at $T = 175$ K than for $N = 1$ at the comparable temperature $T = 170$ K, indicating that the groove promotion begins at a lower temperatures for the interacting $N = 9$ than for the noninteracting $N = 1$.

---

* Electronic address: nurban@phys.psu.edu
† Electronic address: gatica@phys.psu.edu
‡ Electronic address: mwc@psu.edu
§ Electronic address: jlr@unsl.edu.ar
[1] O. Byl, P. Kondratyuk, S. Forth, S. FitzGerald, J.T. Yates, Jr., L. Chen, and J.K. Johnson, J. Amer. Chem. Soc. **125**, 5889 (2003).
[2] M. Bienfait, P. Zeppenfeld, N. Dupont-Pavlovsky, M. Muris, M.R. Johnson, T. Wilson, M. DePies, and O.E. Vilches, Phys. Rev. B **70**, 035410 (2004).
[3] M. Bienfait, P. Zeppenfeld, N. Dupont-Pavlovsky, J.-P. Palmari, M.R. Johnson, T. Wilson, M. DePies, and O.E. Vilches, Phys. Rev. Lett. **91**, 035503 (2003).
[4] Z.J. Jakubek and B. Simard, Langmuir **20**, 5940 (2004).
[5] S. Talapatra, V. Krungleviciute, and A.D. Migone, Phys. Rev. Lett. **89**, 246106 (2002).
[6] S. Talapatra and A.D. Migone, Phys. Rev. B **65**, 045416 (2002).
[7] S. Talapatra, D.S. Rawat, and A.D. Migone, J. Nanosci. Nanotech. **2**, 467 (2002).

[8] B.K. Pradhan, A. Harutyunyan, M. Cole, D. Stojkovic, J.C. Grossman, P. Zhang, V. Crespi, H. Goto, J. Fujiwara, and P.C. Eklund, J. Mater. Res. **17**, 2209 (2002).

[9] S. Ramachandran, T.A. Wilson, D. Vandervelde, D.K. Holmes, and O.E. Vilches, J. Low Temp. Phys. **134**, 115 (2004).

[10] Y.H. Kahng, R.B. Hallock, and E. Dujardin, Physica B **329**, 280 (2003).

[11] T. Wilson, A. Tyburski, M.R. DePies, and O.E. Vilches, J. Low Temp. Phys. **126**, 403 (2002).

[12] T. Wilson, Ph.D. thesis, University of Washington, 2004 (unpublished).

[13] S.M. Gatica, M.J. Bojan, M.W. Cole, M.M. Calbi, and J.K. Johnson (unpublished)

[14] A.D. Migone (unpublished); A.D. Migone and S. Talapatra, in *The Encyclopedia of Nanoscience and Nanotechnology*, edited by H.S. Nalwa (American Scientific, Stevenson Ranch, CA, 2004).

[15] B.W. Smith, R.M. Russo, S.B. Chikkannanavar, and D.E. Luzzi, J. Appl. Phys. **91**, 9333 (2002).

[16] M.R. Smith, Jr., E.W. Bittner, W. Shi, J.K. Johnson, and B.C. Bockrath, J. Phys. Chem. B **107**, 3752 (2003).

[17] J.C. Lasjaunias, K. Biljaković, J.L. Sauvajol, and P. Monceau, Phys. Rev. Lett. **91**, 025901 (2003).

[18] A. Šiber, Phys. Rev. B **66**, 235414 (2002).

[19] A. Kuznetsova, J.T. Yates, Jr., V.V. Simonyan, J.K. Johnson, C.B. Huffman, and R.E. Smalley, J. Chem. Phys. **115**, 6691 (2001).

[20] W. Shi and J.K. Johnson, Phys. Rev. Lett. **91**, 015504 (2003); M.M. Calbi, F. Toigo, and M.W. Cole, cond-mat/0406521 (unpublished); M.R. Johnson, S. Rols, P. Wass, M. Muris, M. Bienfait, P. Zeppenfeld, and N. Dupont-Pavlovsky, Chem. Phys. **293**, 217 (2003).

[21] M.M. Calbi, S.M. Gatica, M.J. Bojan, G. Stan, and M.W. Cole, Rev. Mod. Phys. **73**, 857 (2001); M.M. Calbi, S.M. Gatica, M.J. Bojan, and M.W. Cole, J. Chem. Phys. **115**, 9975 (2001); L. Brualla and M.C. Gordillo, Phys. Rev. B **68**, 075423 (2003).

[22] J.G. Dash, M. Schick, and O.E. Vilches, Surf. Sci. **299/300**, 405 (1994).

[23] L.W. Bruch, M.W. Cole, and E. Zaremba, *Physical Adsorption: Forces and Phenomena* (Oxford University Press, New York, 1997), Chap. 6.

[24] P. Taborek and L. Senator, Phys. Rev. Lett. **57**, 218 (1986).

[25] E.S. Hernández, M.W. Cole, and M. Boninsegni, Phys. Rev. B **68**, 125418 (2003).

[26] S.M. Gatica, M.J. Bojan, G. Stan, and M.W. Cole, J. Chem. Phys. **114**, 3765 (2001).

[27] R.L. Elgin and D.L. Goodstein, Phys. Rev. A **9**, 2657 (1974).

[28] N. Metropolis, A.W. Rosenbluth, M.N. Rosenbluth, A.H. Teller, and E. Teller, J. Chem. Phys. **21**, 1087 (1953).

[29] D. Frenkel and B. Smit, *Understanding Molecular Simulation: From Algorithms to Application* (Academic, New York, 2002).

[30] F. Wang and D.P. Landau, Phys. Rev. Lett. **86**, 2050 (2001).

[31] F. Wang and D.P. Landau, Phys. Rev. E **64**, 056101 (2001).

[32] D.P. Landau, S.-H. Tsai, and M. Exler, Am. J. Phys. **72**, 10 (2004).

[33] B.J. Schulz, K. Binder, M. Müller, and D.P. Landau, Phys. Rev. E **67**, 067102 (2003).

[34] M.S. Shell, P.G. Debenedetti, and A.Z. Panagiotopoulos, Phys. Rev. E **66**, 056703 (2002).

[35] C. Carraro, Phys. Rev. Lett. **89**, 115702 (2002).

[36] C. Carraro, Phys. Rev. B **61**, R16351 (2000).

[37] M.E. Fisher, Phys. Rev. **162**, 480 (1967).

[38] See analogous transition behavior in other cylindrical environments: R. Radhakrishnan and K.E. Gubbins, Phys. Rev. Lett. **79**, 2847 (1997).

[39] T. Wilson and O.E. Vilches, J. Low Temp. Phys. **29**, 732 (2003).

[40] S.M. Gatica, M.M. Calbi, and M.W. Cole, J. Low Temp. Phys. **133**, 399 (2003).

[41] C.G. Shaw and S.C. Fain, Jr., Surf. Sci. **83**, 1 (1979).

[42] Y. Larher, Surf. Sci. **134**, 469 (1983).

[43] A.D. Migone, Z.R. Li, and M.H.W. Chan, Phys. Rev. Lett. **53**, 810 (1984).

[44] Q.M. Zhang and J.Z. Larese, Phys. Rev. B **43**, 938 (1991).

[45] R.K. Pathria, *Statistical Mechanics* (Butterworth-Heinemann, Oxford, Boston, 1996), Chap. 3.

[46] R.A. Trasca, N. Ferralis, R.D. Diehl, and M.W. Cole, J. Phys.: Condens. Matter **16**, S2911 (2004).

[47] M.M. Calbi and M.W. Cole, Phys. Rev. B **66**, 115413 (2002).

[48] A. Šiber, Phys. Rev. B **66**, 205406 (2002).

[49] A. Šiber, Phys. Rev. B **67**, 165426 (2003).

[50] M.K. Kostov, M.M. Calbi, and M.W. Cole, Phys. Rev. B **68**, 245403 (2003).

[51] Q. Wang and J.K. Johnson, Fluid Phase Equilibria **132**, 93 (1997).